Zitierweise: Angew. Chem. Int. Ed. 2025, e202423626
doi.org/10.1002/anie.202423626

Nitrobenzene Hydrogenation

Efficient Generation of Negative Hydrogen with Bimetallic-Ternary-Structured Catalysts for Nitrobenzene Hydrogenation

Ji Shen[+], Minhao Tang[+], Zuhao Shi[+], Shuyan Guan, Yijie Shi, Zechao Zhuang, Runze Li, Jiarui Yang, Daping He,* Baozhong Liu,* Yuhai Dou, and Dingsheng Wang**

Abstract: Transition metal-catalyzed transfer hydrogenation (TH) with in situ negative hydrogen (H^-) has received extensive attention as an alternative to conventional high-pressure hydrogenation processes. However, the insufficient activity of hydrogen production and unclear the conversion process of hydrogenation remain a great challenge. In this work, brand new bimetallic ternary-structured catalysts ($Ru_{1+n}M_1$-TiO_2, M=Co, Cu, Fe, Ni) were synthesized to efficiently generate H^- donors from ammonia borane (AB, NH_3BH_3) for nitrobenzene hydrogenation under moderate conditions. The $Ru_{1+n}Co_1$-TiO_2 catalysts exhibited highest activity for hydrogen production form AB hydrolysis with a TOF value of 2716 min^{-1}. The $Ru_{1+n}Co_1$-TiO_2 achieved >90 % yields within 3–4 hours in converting nitrobenzene to anilines using AB. Mechanistic studies revealed that the high hydrolysis activity was due to that the Ru SA and Co SA sites of the bimetallic-ternary-structured catalyst required the lowest energy for the activation of AB and H_2O, respectively. Remarkably, the Co SA and Ru clusters exhibited an obvious synergistic effect in the TH process, which promoted the tandem hydrogenation of nitroaromatics. This work demonstrated an efficient approach to generate H^- donor with bimetallic-ternary-structured catalysts in TH process and further provided new inspiration on the development of multifunctional catalysts.

Introduction

Transfer hydrogenation (TH) has been regarded as one of the most important and fundamental transformations used in chemistry[1]. The direct addition of H_2 to unsaturated groups is a well-developed area of reduction chemistry, which makes gaseous H_2 the preferred source of hydrogen in many of these transformations[2]. Typically, reactions with molecular gaseous hydrogen require specialized equipment for pressurization and heating operations, which raises a number of safety issues[3]. Other hydrogen storage media such as formic acid, methanol, ammonia, ethanol have flammable, corrosive properties and easily harm the environment as shown in Figure 1a[4]. Ammonia borane (AB, NH_3BH_3) has the advantage of low molecular weight (30.87 g mol^{-1}), high hydrogen content (19.6 % wt %)[5], and is considered as promising alternatives to TH agents[6]. AB has been employed as a hydrogen supply source in organic reductive transformations because of high hydrogen density, non-toxicity, safety, controllability, convenience, and unrestricted sites as well as ease of transport and storage[7,8]. AB-TH can be carried out under relatively mild conditions and usually does not require high-temperature and high-pressure reaction conditions, which makes the reactants easy to handle. Meanwhile, AB is also being progressively regenerated in a number of feasible ways to reduce its cost, such as regeneration of AB using hydrazine and liquid ammonia, regeneration of AB by hydrodechlorination, regeneration of AB with lithium aluminum hydride[6c,9].

However, the TH process using AB for in situ generation of negative hydrogen (H^-) donors still has two main problems as follows, one of which is that the hydrolysis of

[*] J. Shen,[+] Dr. S. Guan, Y. Shi, Dr. Z. Zhuang, R. Li, J. Yang, Prof. D. Wang
Engineering Research Center of Advanced Rare Earth Materials, Department of Chemistry
Tsinghua University
Beijing 100084, China
E-mail: guanshuyan@mail.tsinghua.edu.cn
wangdingsheng@mail.tsinghua.edu.cn

M. Tang[+]
Beijing National Laboratory for Molecular Sciences, CAS Laboratory of Colloid and Interface and Thermodynamics, CAS Research/Education Center for Excellence in Molecular Sciences, Center for Carbon Neutral Chemistry
Institute of Chemistry, Chinese Academy of Sciences
Beijing 100190, China

Z. Shi,[+] Prof. D. He
School of Physics and Mechanics, Wuhan University of Technology
Wuhan 430070, China
E-mail: hedaping@whut.edu.cn

Prof. B. Liu
College of Chemistry and Chemical Engineering, State Collaborative Innovation Center of Coal Work Safety and Clean-efficiency Utilization
Henan Polytechnic University
Jiaozuo 454000, China
E-mail: bzliu@hpu.edu.cn

Prof. Y. Dou
Institute of Energy Materials Science
University of Shanghai for Science and Technology
Shanghai 200093, China

[+] These authors contributed equally to this work.

© 2025 Wiley-VCH GmbH

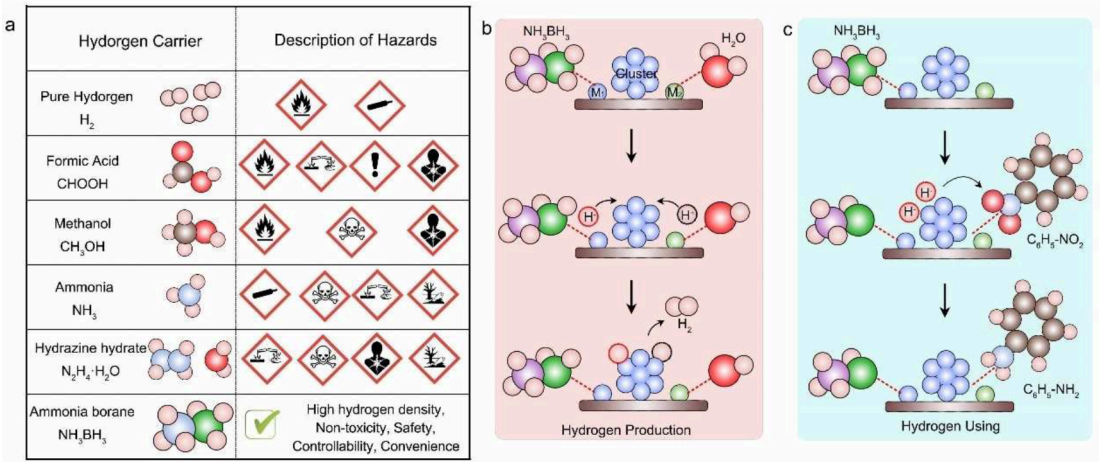

Figure 1. (a) The advantage of AB compared with other hydrogen carrier. Schematic diagram of (b) AB hydrolysis and (c) tandem hydrogenation of nitrobenzene by coupling with AB as H^- donors on bimetallic-ternary-structured catalysts $Ru_{1+n}M_n$-TiO_2.

AB requires highly efficient catalysts, and the activity of the current single metal catalysts Ru[10], Rh[11], Pt[12], Pd[13] still needs to be further improved[14]. Single noble metal is not only expensive, but also more difficult for many multi-step activation steps of the AB hydrolysis reaction, either in clusters or single-atom[15]. The second is that the conversion process of hydrogen generation is not clear and still requires rational design of simple experiments to be used as probes to confirm the hydrogenation pathway, as well as computational analyses to confirm the reaction mechanism[16]. Therefore, the catalyst structure needs to be rationally designed to meet the multi-step activation process[17], and sophisticated in situ characterization should also be used for the study of TH processes. It is a very effective way for integrating multi-sites such as single atom (SA) and clusters to build synergistic catalytic sites for improving the conversion efficiency of hydrogenation[18]. For example, in the (PtRu/pN–C) catalyst, Ru optimizes the hydrogen binding energy by modulating the electronic structure of Pt, while the Pt single atom on pN–C optimizes the interfacial water structure[19]. Also, constructing multi-site catalysts can increase the stability for the hydrogenation process[20]. Therefore, the integration of multi-sites in a single system, which can take advantage of the electron transfer and synergistic interactions between different sites and is of great significance in optimizing the catalytic performance.

We aimed to assemble a multi-site catalyst, each site tailored for a specific role in an efficient multi-step catalytic process. In the AB hydrolysis reaction, the M_1 SA site was responsible for the activation of H^- in the B–H bond, and the M_2 SA site was responsible for the breakage of H^+in the O–H bond, and the activated H^- and H^+on the cluster combined to form H_2 and desorbed (Figure 1b). In the tandem hydrogenation reaction of nitrobenzene, the H^- in the AB molecule (as the H^- donor) remained dissociated at the M_1 SA site, the dissociated H^- transferred to clusters and M_2 SA and then combined with nitrobenzene to form aniline (Figure 1c).

In this work, we reported a general and reliable strategy to synthesize bimetallic-ternary-structured catalysts ($Ru_{1+n}M_1$-TiO_2, M=Co, Cu, Fe, Ni) consisting of defined clusters and SA sites via a simple impregnation reduction method. The optimized $Ru_{1+n}Co_1$-TiO_2 exhibited excellent AB dehydrogenation performance with a TOF value of 2716 min^{-1}, superior to most noble metal catalysts. Interestingly, the boosting effect had been observed in tandem hydrogenation of nitrobenzene by coupling with AB as H^- donors over $Ru_{1+n}Co_1$-TiO_2 catalysts. This $Ru_{1+n}Co_1$-TiO_2 greatly increased the catalytic conversion (>99 %) in hydrogenation of nitrobenzene to aniline outperforming the samples with $Ru_{1+n}Cu_1$-TiO_2 and Ru_n-TiO_2. In addition, the intermediate C_6H_5-NO* was captured by in situ Raman spectra and the reliability of mechanism was proved by DFT calculations. This study not only demonstrated the effectiveness of bimetallic-ternary-structured catalysts with cluster-single atom for hydrogen generation from chemical hydrogen storage materials, but also paved the way for synergistically promoting TH process.

Results and Discussion

Formation of Catalyst and Characterization Of Bimetallic-Ternary Structure

We initially synthesized the RuCo catalysts on TiO_2 support using the wetness impregnation method. Specifically, a certain molar amount of $RuCl_3{\cdot}xH_2O$ and $Co(NO_3)_2{\cdot}6H_2O$ was added to the TiO_2 solution and stirred for 24 h, washed and dried, and then further treated in 5 % H_2/Ar_2 at 350 °C for 3 h to obtain the desired catalyst. The obtain catalysts were designated as $Ru_{1+n}Co_1$-TiO_2. In addition, the TiO_2 supported $Ru_{1+n}M_1$ (M= Mn, Co, Ni, Cu) and only Ru were prepared as well for comparison, the mass ratio was measured by inductively coupled plasma optical emission spectrometer (ICP-OES, Table S1).

© 2025 Wiley-VCH GmbH

15213757, 2025, 0, Downloaded from https://onlinelibrary.wiley.com/doi/10.1002/ange.202423626. By WUHAN UNIVERSITY OF TECHNOLOGY, Wiley Online Library on [30/03/2025]. See the Terms and Conditions (https://onlinelibrary.wiley.com/terms-and-conditions) on Wiley Online Library for rules of use; OA articles are governed by the applicable Creative Commons License

The morphology of $Ru_{1+n}Co_1$-TiO_2, $Ru_{1+n}Cu_1$-TiO_2, $Ru_{1+n}Mn_1$-TiO_2, $Ru_{1+n}Ni_1$-TiO_2, Ru_n-TiO_2 catalysts were investigated by aberration corrected high angle annular dark field scanning transmission electron microscopy (AC HAADF-STEM) and high-resolution transmission electron microscopy (HR-TEM) images. By calcining the precursors of Ru and Co metals together, the bimetallic-ternary structure with coexistence of Co SA, Ru SA and Ru cluster was formed during the pyrolysis process, which was confirmed in the AC HAADF-STEM images at different magnifications (Figure 2a, b). In addition, energy dispersive X-ray spectroscopy (EDS, Figure 2c) elemental mapping analysis provided conclusive evidence for the uniform distribution of Co SAs on the TiO_2 surface, while Ru exhibited both SAs and cluster on the TiO_2 surface. Likewise, similar to $Ru_{1+n}Co_1$-TiO_2, the AC HAADF-STEM, HR-TEM images and EDS of $Ru_{1+n}Cu_1$-TiO_2, $Ru_{1+n}Mn_1$-TiO_2, $Ru_{1+n}Ni_1$-TiO_2 (Figure 2d~f, Figure S1, 2) similarly demonstrated the formation of Cu/Mn/Ni SA, Ru SA and Ru cluster coexistence. The above results indicated that the bimetallic-ternary-structured catalysts $Ru_{1+n}M_n$-TiO_2 were successfully synthesized. However, differing from the $Ru_{1+n}M_n$-TiO_2, Ru atoms of Ru_n-TiO_2 were spotted anchoring on the TiO_2 support with the form of clusters, as shown by the higher-magnification AC HAADF-STEM image and corresponding 3D fitting map (Figure 2g~j). And, the enlarged HAADF-STEM image revealed that Ru clusters with an average particle size of 2–3 nm were uniformly distributed on the surface of the TiO_2 support.

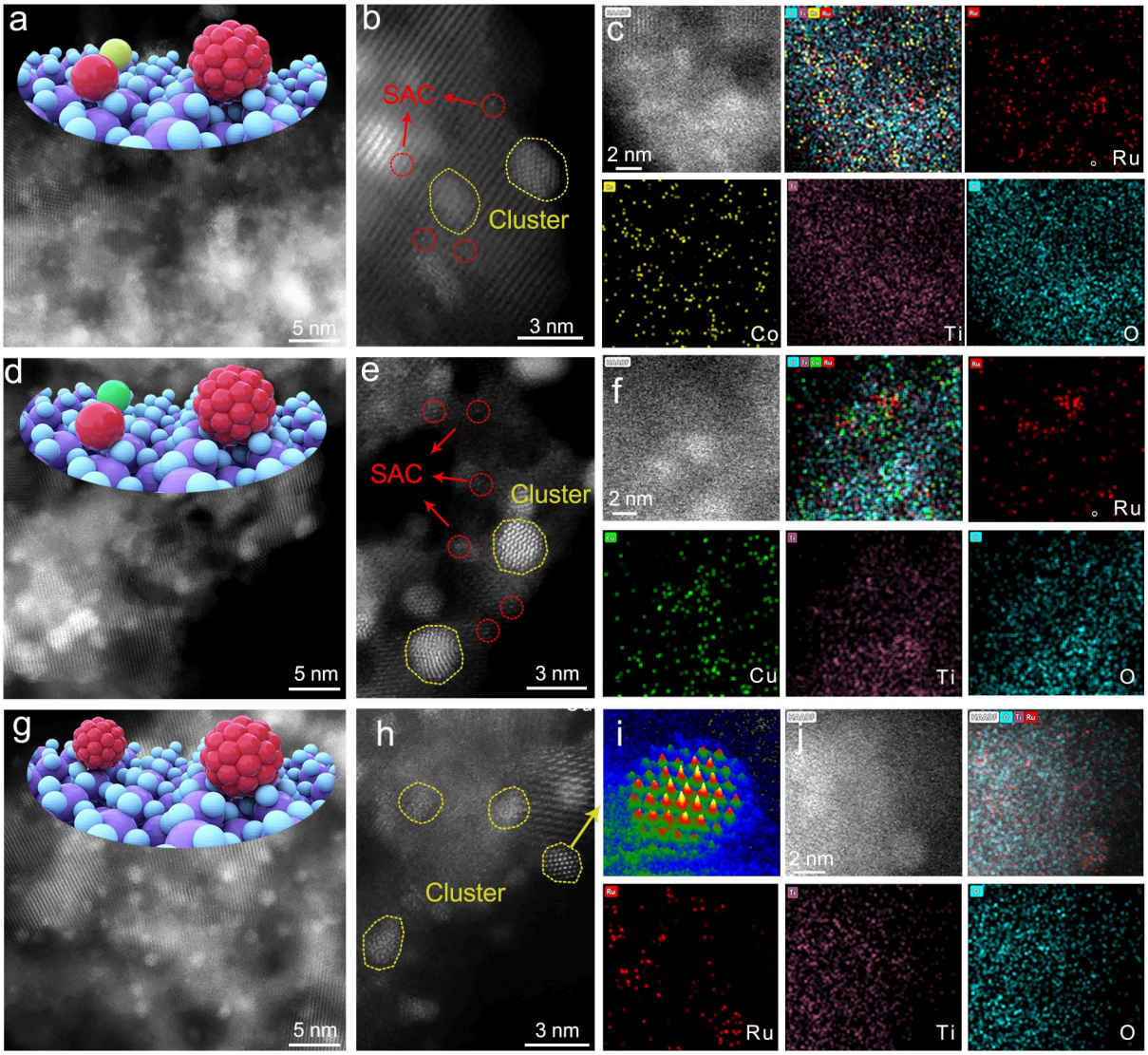

Figure 2. (a) AC-HAADF-STEM image of $Ru_{1+n}Co_1$-TiO_2 catalyst. (b) The AC-HAADF-STEM image of $Ru_{1+n}Co_1$-TiO_2 catalyst at high magnification. (c) The corresponding EDS elemental mapping $Ru_{1+n}Co_1$-TiO_2. (d) AC-HAADF-STEM image of $Ru_{1+n}Cu_1$-TiO_2 catalyst. (e) The AC-HAADF-STEM image of $Ru_{1+n}Cu_1$-TiO_2 catalyst at high magnification. (f) The corresponding EDS elemental mapping $Ru_{1+n}Cu_1$-TiO_2. (g) AC-HAADF-STEM image of Ru_n-TiO_2 catalyst. (h) The AC-HAADF-STEM image of Ru_n-TiO_2 catalyst at high magnification. (i) A 3D fitting map of the yellow dashed area of Ru_n-TiO_2 catalyst. (j) The corresponding EDS elemental mapping Ru_n-TiO_2.

© 2025 Wiley-VCH GmbH

15213757, 2025, 0, Downloaded from https://onlinelibrary.wiley.com/doi/10.1002/ange.202423626. By WUHAN UNIVERSITY OF TECHNOLOGY, Wiley Online Library on [30/03/2025]. See the Terms and Conditions (https://onlinelibrary.wiley.com/terms-and-conditions) on Wiley Online Library for rules of use; OA articles are governed by the applicable Creative Commons License

To gain insight into the bimetallic-ternary-structured catalysts, the refined structures of the as-synthesized $Ru_{1+n}Co_1$-TiO_2 catalysts were systematically characterized by typical X-ray spectroscopy techniques. The X-ray spectroscopy technique (XRD) spectra of all the prepared catalysts showed only characteristic peaks associated with anatase TiO_2 (Figure S3), suggesting that the presence of single atoms or small clusters had little effect on the crystal structure of the TiO_2 support. Concomitantly, X-ray photoelectron spectroscopy (XPS) analysis of these catalysts also unveiled electronic structures of bimetallic-ternary catalysts. Specifically, the valence state of Co in $Ru_{1+n}Co_1$-TiO_2 was analyzed by Co 2p spectroscopy with peaks at ~781.3 and 796.8 eV corresponding to 2p 3/2 and 2p 1/2 of Co (Figure 3a). The XPS peaks that appeared at ~932.5 and 952.1 eV correspond to the orbitals of the Cu species in the

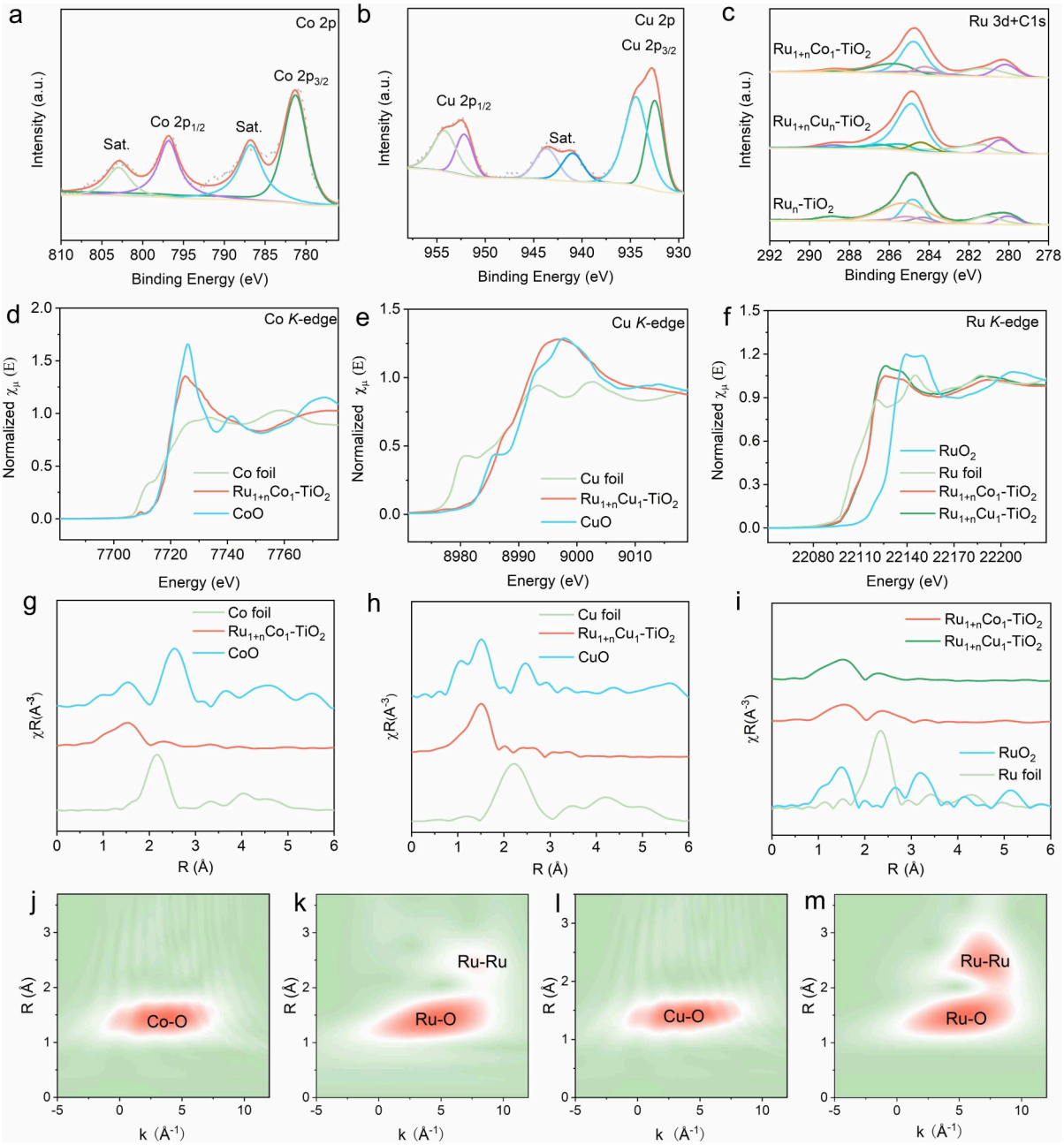

Figure 3. Structure characterizations of catalysts. (a) Co 2p XPS spectra of $Ru_{1+n}Co_1$-TiO_2, (b) Cu 2p XPS spectra of $Ru_{1+n}Cu_1$-TiO_2, (c) Ru 3d+C 1s XPS spectra of $Ru_{1+n}Co_1$-TiO_2, $Ru_{1+n}Cu_1$-TiO_2 and Ru_n-TiO_2. (d) Normalized XANES spectra at Co K-edge of $Ru_{1+n}Co_1$-TiO_2, Co foil and CoO. (e) Normalized XANES spectra at Cu K-edge of $Ru_{1+n}Cu_1$-TiO_2, Cu foil and CuO. (f) Normalized XANES spectra at Ru K-edge of $Ru_{1+n}Co_1$-TiO_2, $Ru_{1+n}Cu_1$-TiO_2, Ru foil and RuO_2. (g) Co K-edge EXAFS spectra in the R space for $Ru_{1+n}Co_1$-TiO_2, Co foil and CoO. (h) Cu K-edge EXAFS spectra in the R space for $Ru_{1+n}Cu_1$-TiO_2, Cu foil and CuO. (i) Ru K-edge EXAFS spectra in the R space for $Ru_{1+n}Co_1$-TiO_2, $Ru_{1+n}Cu_1$-TiO2, Ru foil and RuO_2. 2D contour plots of WT-XAFS spectra: (j) Co in $Ru_{1+n}Co_1$-TiO_2, (k) Ru in $Ru_{1+n}Co_1$-TiO_2 (l) Cu in $Ru_{1+n}Cu_1$-TiO_2, (m) Ru in $Ru_{1+n}Cu_1$-TiO_2.

© 2025 Wiley-VCH GmbH

15213757, 2025, 0, Downloaded from https://onlinelibrary.wiley.com/doi/10.1002/ange.202423626. By WUHAN UNIVERSITY OF TECHNOLOGY, Wiley Online Library on [30/03/2025]. See the Terms and Conditions (https://onlinelibrary.wiley.com/terms-and-conditions) on Wiley Online Library for rules of use; OA articles are governed by the applicable Creative Commons License

$Ru_{1+n}Cu_1$-TiO_2 catalyst (Figure 3b). Evidently, the Ru 3d binding energy in the $Ru_{1+n}Co_1$-TiO_2 and $Ru_{1+n}Cu_1$-TiO_2 samples showed a positive shift compared to the Ru_n-TiO_2 catalyst, which should be ascribed to the electron transfer between Ru and second metal Co, Cu (Figure 3c). Additionally, the Ti 2p XPS spectra of $Ru_{1+n}Co_1$-TiO_2 and $Ru_{1+n}Cu_1$-TiO_2, and Ru_n-TiO_2 catalyst exhibited congruent binding energy at ~458.7 and 464.4 eV (Figure S4), and the peak at binding energy of ~530.1 and 531.5 eV attributed to O 1s XPS spectra of the three samples (Figure S5).

X-ray absorption fine structure (XAFS) measurements were carried out to examine the atomic dispersion and geometric configuration of the $Ru_{1+n}Co_1$-TiO_2 and $Ru_{1+n}Cu_1$-TiO_2 catalyst. In the Co and Cu K-edge X-ray absorption near edge structure (XANES) curves, the oxidation state of Co and Cu in $Ru_{1+n}Co_1$-TiO_2 and $Ru_{1+n}Cu_1$-TiO_2 were closed to the +2-valence state, as indicated by the position of the K-edge spectral line closing to the K edge spectral line of CoO/CuO (Figure 3d, e). The Ru K-edge XANES spectra recorded that the white-line peak of $Ru_{1+n}Co_1$-TiO_2 and $Ru_{1+n}Cu_1$-TiO_2 located between Ru foil and RuO_2, closer to the 0-valence state, indicating that Ru atoms existed in SA and metallic state (Figure 3f).

Fourier transform extended X-ray absorption fine structure (FT-EXAFS) had been conducted in order to further reveal the bonding information and fine coordination structure of the catalyst surface. The *k*-space spectrum was obtained by k^2-weight EXAFS (Figure S6~8). The R-space spectra were obtained after Fourier transform for characterizing the bonding information of Ru, Co, Cu with surrounding atoms in $Ru_{1+n}Co_1$-TiO_2 and $Ru_{1+n}Cu_1$-TiO_2. The peak at 1.5 Å was only present in $Ru_{1+n}Co_1$-TiO_2 and $Ru_{1+n}Cu_1$-TiO_2, this signal was attributed to the contribution of Co–O/Cu–O coordination (Figure 3g, h). While in both Co foil and Cu foil spectra, it displayed a main peak at approximately 2.5 Å assigned to the Co–Co/Cu–Cu path. Thus, this Co and Cu metallic interaction was not present in the synthesized catalysts, consistent with the existence of Co and Cu single atoms. Whereas the presence of Ru–O peak at 1.4 Å and Ru–Ru peak at 2.3 Å in $Ru_{1+n}Co_1$-TiO_2 and $Ru_{1+n}Cu_1$-TiO_2 further suggested the coexistence of Ru SA and Ru small clusters (Figure 3i). By EXAFS fitting (Figure S9~15), both Cu and Co atoms were coordinated with 2 O in the first shell layer, as well as 2 O around the Ru SA, and the corresponding fitting parameters were shown in Table S2. In addition, the wavelet transform (WT) could be used as a complement to FT-EXAFS to identify the microstructure of catalysts due to its strong resolution in both *k* and R spaces. As shown in Figure 3j~m, Figure S16~18, the 2D WT contour plots of Co/Cu SA in the $Ru_{1+n}Co_1$-TiO_2 and $Ru_{1+n}Cu_1$-TiO_2 samples did not have metallic bonding scattering paths compared to Co/Cu foil. The 2D WT contour plots of $Ru_{1+n}Co_1$-TiO_2 and $Ru_{1+n}Cu_1$-TiO_2 had Ru–O scattering paths and had Ru–Ru scattering paths in contrast to Ru foil and RuO_2. The above analysis of the XAS results confirmed that the $Ru_{1+n}Co_1$-TiO_2 and $Ru_{1+n}Cu_1$-TiO_2 catalysts are all coexisting as Ru, Co/Cu SAs as well as Ru clusters.

Catalytic Activity of $Ru_{1+n}M_1$-TiO_2 in AB Hydrolysis

The dehydrogenation of AB hydrolysis for $Ru_{1+n}M_1$-TiO_2 catalysts was evaluated by drainage methods in a batch reactor with constant pressure separating funnel. As shown in Figure 4a, the times of complete dehydrogenation for AB hydrolysis using $Ru_{1+n}Co_1$-TiO_2, $Ru_{1+n}Cu_1$-TiO_2, Ru_n-TiO_2, $Ru_{1+n}Mn_1$-TiO_2 and $Ru_{1+n}Ni_1$-TiO_2 were 4.8, 4.5, 7.1, 8.3 and 10.5 min, respectively. The corresponding TOF of $Ru_{1+n}Co_1$-TiO_2, $Ru_{1+n}Cu_1$-TiO_2, Ru_n-TiO_2, $Ru_{1+n}Mn_1$-TiO_2 and $Ru_{1+n}Ni_1$-TiO_2 were 2716, 2467, 1796, 1437, 666 min^{-1}, respectively (Figure 4b). To investigate the kinetics of AB hydrolysis dehydrogenation of bimetallic-ternary-structured catalysts, the kinetic experiments on $Ru_{1+n}Co_1$-TiO_2, $Ru_{1+n}Cu_1$-TiO_2 and Ru_n-TiO_2 catalysts in the temperature range of 298, 303, 308 K were performed (Figure 4c, Figure S19~21). When the temperature was increased from 298 to 308 K, the *TOF* of $Ru_{1+n}Co_1$-TiO_2, $Ru_{1+n}Cu_1$-TiO_2 and Ru_n-TiO_2 increased from 2716 to 4414 min^{-1}, 2467 to 3880 min^{-1}, 1545 to 2746 min^{-1}. The lower thermal activation energies E_a (Figure 4d) of $Ru_{1+n}Co_1$-TiO_2 (37.06 kJ mol^{-1}) also confirmed its structural advantage for accelerating AB hydrolysis compared with $Ru_{1+n}Cu_1$-TiO_2 (34.50 kJ mol^{-1}) and Ru_n-TiO_2 (43.9 kJ mol^{-1}). The catalytic activity of $Ru_{1+n}Co_1$-TiO_2 caught up with the highest level compared to those reported noble-based catalysts (Figure 4e, Table S3). In order to investigate the synergistic effect, the hydrogen production activity of $Ru_{1+n}Co_1$-TiO_2, $Ru_{1+n}Cu_1$-TiO_2 and physical mixture catalyst Ru_n-TiO_2 + Co_1-TiO_2, Ru_n-TiO_2 + Cu_1-TiO_2 was compared. As shown in Figure S22, the times of complete dehydrogenation for AB hydrolysis using $Ru_{1+n}Co_1$-TiO_2, and Ru_n-TiO_2 + Co_1-TiO_2, $Ru_{1+n}Cu_1$-TiO_2, and Ru_n-TiO_2 + Cu_1-TiO_2 were 4.8, 23.2, 4.5, 18.3 min, respectively. The complete hydrogen production time for AB hydrolysis on the $Ru_{1+n}Co_1$-TiO_2 catalyst was five times higher than that on the Ru_n-TiO_2 + Co_1-TiO_2 physical hybrid catalyst, respectively. And, different ratios of RuCo-TiO_2 were synthesized to compare their catalytic properties. As shown in Figure S23, the times of complete dehydrogenation for AB hydrolysis using bimetallic-ternary-structured catalysts $Ru_{2*(1+n)}Co_1$-TiO_2, $Ru_{1+n}Co_{2*1}$-TiO_2, $Ru_{1+n}Co_1$-TiO_2, $Ru_{0.5*(1+n)}Co_1$-TiO_2, $Ru_{1+n}Co_{0.5*1}$-TiO_2 were 3.4, 4.3, 4.5, 7.9 and 9.9 min, respectively. Increasing or decreasing the amount of Ru had a greater effect on the hydrogen production than increasing or decreasing the amount of Co.

The time plot of hydrogen evolution versus various concentration of AB with $Ru_{1+n}Co_1$-TiO_2 catalyst was shown in Figure S24a. The hydrogen volume increased with increasing AB concentration, but the rate of hydrogen evolution rised insignificantly (Figure S24b). The corresponding logarithmic plot had a 0.192 slope, indicating close zero-order reaction for the concentration of AB (Figure S24c). ^1H and ^{11}B nuclear magnetic resonance (NMR) spectroscopy showed that the products in aqueous solution were NH_4^+ and BO_2^-, further verifying the complete hydrolysis of AB using $Ru_{1+n}Co_1$-TiO_2 catalyst (Figure S25 and S26).

© 2025 Wiley-VCH GmbH

15213757, 2025, 0, Downloaded from https://onlinelibrary.wiley.com/doi/10.1002/ange.202423626. By WUHAN UNIVERSITY OF TECHNOLOGY, Wiley Online Library on [30/03/2025]. See the Terms and Conditions (https://onlinelibrary.wiley.com/terms-and-conditions) on Wiley Online Library for rules of use; OA articles are governed by the applicable Creative Commons License

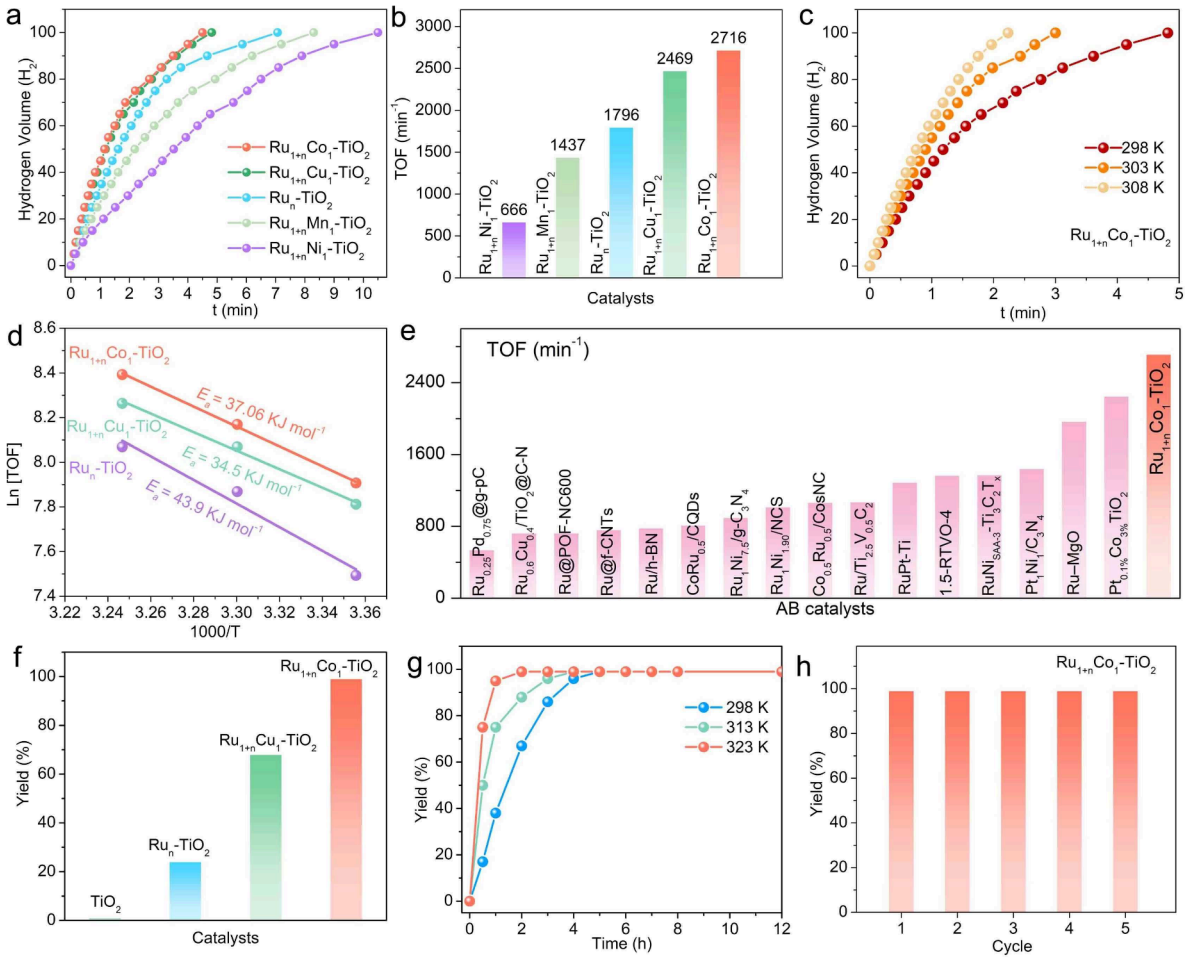

Figure 4. (a) The curve of hydrogen generation for different active site structures $Ru_{1+n}Co_1$-TiO_2, $Ru_{1+n}Cu_1$-TiO_2, Ru_n-TiO_2, $Ru_{1+n}Mn_1$-TiO_2 and $Ru_{1+n}Ni_1$-TiO_2. (b) the comparison *TOF* for $Ru_{1+n}Co_1$-TiO_2, $Ru_{1+n}Cu_1$-TiO_2, Ru_n-TiO_2, $Ru_{1+n}Mn_1$-TiO_2 and $Ru_{1+n}Ni_1$-TiO_2. (c) The curve of hydrogen of $Ru_{1+n}Co_1$-TiO_2 for different temperature 298 K, 303 K, 308 K. (d) The E_a for $Ru_{1+n}Co_1$-TiO_2, $Ru_{1+n}Cu_1$-TiO_2, and Ru_n-TiO_2.. (e) TOF of $Ru_{1+n}Co_1$-TiO_2 and recently Ru-based catalysts for AB hydrolysis. (f) Catalyst activity for converting nitrobenzene into aniline. (g) Yield versus reaction time of $Ru_{1+n}Co_1$-TiO_2 catalyzed hydrogenation of nitrobenzene to aniline at different temperatures. (h) Stability of $Ru_{1+n}Co_1$-TiO_2 in TH process in 8 h. Reaction condition: $Ru_{1+n}Co_1$-TiO_2 10 mg, substrate 1 mmol, NH_3BH_3 92 mg, CH_3OH 2 mL, H_2O 0.1 g, 313 K, 8 h.

Catalytic Activity of $Ru_{1+n}M_1$-TiO_2 in the AB-TH to Nitroaromatics

The catalysts $Ru_{1+n}Co_1$-TiO_2, $Ru_{1+n}Cu_1$-TiO_2 and Ru_n-TiO_2 were then investigated for the AB-TH to a variety of nitrobenzene derivative. To this aim, nitrobenzene was selected to optimize the AB-TH conditions with $Ru_{1+n}Co_1$-TiO_2 catalyst. The activities of the resultant catalysts were examined in conversion of nitrobenzene into aniline using negative hydrogen in situ in place of gas tank hydrogen. The catalyst $Ru_{1+n}Co_1$-TiO_2 was very effective in converting nitrobenzene into aniline in high yields of 99 %, outperforming than those using $Ru_{1+n}Cu_1$-TiO_2 or Ru_n-TiO_2 as catalyst under the same experimental conditions (Figure 4f). The higher aniline yield of $Ru_{1+n}Co_1$-TiO_2 was initially attributed to the stronger synergistic effect between the Ru and Co sites of the metal, which was more favorable for interaction with the intermediates. In order to better illustrate the stronger synergistic effect between the Ru and Co sites, the performances of different ratios of RuCo-TiO_2 and RuCu-TiO_2 catalysts for AB-TH to nitrobenzene hydrogenation were compared (Figure S27). We could find that the catalytic activity of any proportion of RuCo-TiO_2 was higher than the catalytic activity of the same proportion of RuCu-TiO_2. To obtain information on the oxidation states of Co of $Ru_{1+n}Co_1$-TiO_2 and Cu of $Ru_{1+n}Cu_1$-TiO_2 throughout the reaction, in situ XPS was performed (Figure S28, 29). From the in situ XPS spectra of Co 2p of $Ru_{1+n}Co_1$-TiO_2, Co SA in $Ru_{1+n}Co_1$-TiO_2 did not change significantly throughout the reaction; whereas Cu SA in $Ru_{1+n}Cu_1$-TiO_2 was reduced from $Cu^{2+}$to Cu^{+}during the first step of AB dissociation, and the Cu species were still present as Cu+during the second step of nitrobenzene hydrogenation. Based on the XPS results, in situ XAFS analysis of $Ru_{1+n}Co_1$-TiO_2 was further performed (Figure S30). From the XANES results, we could see that Co SA remains in the +2 valence state throughout the reaction. From the EXAFS results, the peak of $Ru_{1+n}Co_1$-TiO_2 exists only at 1.5 Å of Co–O during the

© 2025 Wiley-VCH GmbH

15213757, 2025, 0, Downloaded from https://onlinelibrary.wiley.com/doi/10.1002/ange.202423626. By WUHAN UNIVERSITY OF TECHNOLOGY, Wiley Online Library on [30/03/2025]. See the Terms and Conditions (https://onlinelibrary.wiley.com/terms-and-conditions) on Wiley Online Library for rules of use; OA articles are governed by the applicable Creative Commons License

reaction, and no particles or clusters were formed. Moreover, the structural characterization of $Ru_{1+n}Co_1$-TiO_2 after the reaction was checked. The AC HAADF-STEM and EDS images of $Ru_{1+n}Co_1$-TiO_2 after AB hydrolysis and AB-TH to nitrobenzene hydrogenation were shown in Figure S31, 32. The $Ru_{1+n}Co_1$-TiO_2 did not undergo significant changes and still maintained the coexistence of Co SA, Ru SA and Ru cluster after reaction.Therefore, the datas of in situ XPS, XAFS and AC HAADF-STEM further proved the stable existence of $Ru_{1+n}Co_1$-TiO_2 during reaction process.

The hydrogenation activity of AB-TH to nitrobenzene was aslo compared between $Ru_{1+n}Co_1$-TiO_2, $Ru_{1+n}Cu_1$-TiO_2 and physical mixture catalyst Ru_n-TiO_2 + Co_1-TiO_2, Ru_n-TiO_2 + Cu_1-TiO_2. The yield of converting nitrobenzene into aniline using $Ru_{1+n}Co_1$-TiO_2, and Ru_n-TiO_2 + Co_1-TiO_2, $Ru_{1+n}Cu_1$-TiO_2, and Ru_n-TiO_2 + Cu_1-TiO_2 were 99 %, 33 %, 68 %, 39 %, respectively (Figure S33). The catalytic performance on the $Ru_{1+n}Co_1$-TiO_2 catalyst was three times higher than that on the Ru_n-TiO_2 + Co_1-TiO_2, suggesting that the high activity was mainly dependent on the characteristics of bimetallic-ternary-structured. The catalytic properties of different ratios of RuCo-TiO_2 were displayed in the Figure S34. The increase in Ru loading improved the ability of NH_3BH_3 to produce hydrogen. However, it was possible that H^- was rapidly converted to H_2 and the amount of H^- transferred to nitrobenzene decreased, so the yield of aniline decreased. And the decrease of Ru content made the hydrogen production ability decreased greatly, so the yield of aniline decreased significantly. The change of Co loading changed the electronic state of the catalysts, so it changed the hydrogenation ability of the catalysts. When the temperature increased from 298 to 323 K, the time of complete conversion decreased from 4 to 2 h by $Ru_{1+n}Co_1$-TiO_2 catalyst (Figure 4g).

To demonstrate the role of H^- using AB donors, the process of AB-TH to nitrobenzene hydrogenation was tested by replacing the H source with H_2 (Figure S35). When NH_3BH_3 was used as the H source, the reaction achieved 99 % aniline conversion within 4 h. When H_2 was used as the H source at 0.5 MPa, the reaction achieved only 88 % aniline conversion after a much longer period of time of 12 h. This suggested that the H^- in NH_3BH_3 was more readily transferred to nitrobenzene for subsequent hydrogenation reactions, resulting in higher conversion efficiencies in a shorter period of time. This also proves that the H^- provided by NH_3BH_3 was more conducive to the hydrogenation of nitrobenzene. Additionally, this recovery/recycling test was operated for 5 cycles with >90 % yield remaining unchanged, emphasizing the excellent cycling stability of the catalysts (Figure 4h, Figure S36). Subsequently, the catalyst $Ru_{1+n}Co_1$-TiO_2 was recovered after recycling test and AC HAADF-STEM and EDS tests was performed (Figure S37). The experimental results showed that the morphology of the catalyst after five cycles of testing remained consistent with that before the reaction. Metal Co was present as SA and metal Ru still exhibited SA and cluster coexistence. Taking the optimized conditions in hand, the substrate scope of hydrogenation of nitrobenzene derivative to amine compounds was explored. As shown in Table 1, a variety of nitrobenzene derivative were tested and all of these substrates are well tolerated and converted efficiently to the corresponding amine compounds in high conversion. Aromatic rings with electron withdrawing (halogen and nitro) or electron donating substituents (hydroxyl, methoxy, methyl and amino) in the ortho/meta/para positions could be converted to the corresponding products in near-quantity yields.

Mechanistic studies of TH process

In order to understand the TH process and the origin of activity of the catalysts, the adsorption activation behaviors of $Ru_{1+n}Co_1$-TiO_2, $Ru_{1+n}Cu_1$-TiO_2 and Ru_n-TiO_2 were investigated by using DFT calculations. The structures of the model for $Ru_{1+n}Co_1$-TiO_2, $Ru_{1+n}Cu_1$-TiO_2 and Ru_n-TiO_2 were shown in Figures S38–S40. The Ru SA, Co SA and Ru cluster sites on $Ru_{1+n}Co_1$-TiO_2 were presented in Figure 5a. The Figure 5b showed that the adsorption energies of Co SA, Ru SA, Ru cluster sites for H_2O were −2.74, −2.17, and −1.63 eV and for AB were −2.14, −2.84, and −1.12 eV, respectively. This suggested that the Co SA site and Ru SA site were optimal adsorption sites for H_2O and AB molecules, respectively. The free energy changes of AB and H_2O during B–H and O–H bond breaking process on $Ru_{1+n}Co_1$-TiO_2, $Ru_{1+n}Cu_1$-TiO_2, and Ru_n-TiO_2 were shown in Figure 5c, d. The energy barriers (ΔE) corresponding to the activation of H_2O by $Ru_{1+n}Co_1$-TiO_2, $Ru_{1+n}Cu_1$-TiO_2 and Ru_n-TiO_2 were 0.40, 0.89, 1.99 eV, respectively. The ΔE corresponding to the activation of AB by $Ru_{1+n}Co_1$-TiO_2, $Ru_{1+n}Cu_1$-TiO_2 and Ru_n-TiO_2 were 0.18, 0.23, 1.13 eV, respectively. It was shown that the $Ru_{1+n}Co_1$-TiO_2 catalyst had the best catalytic sites for AB hydrolysis.

In order to obtain further information about the process of AB hydrolysis, the optimal theoretical pathway was simulated. The specific pathways were as follows:

$$S3-S4: NH_3NH_3 + 2H_2O \rightarrow NH_3BH_3 + 2H + 2OH$$

$$S4-S5: NH_3BH_3 + 2H + 2OH \rightarrow NH_3BH_3 + 2OH + H_2\uparrow$$

$$S5-S6: NH_3BH_3 + 2OH \rightarrow NH_3BH_2 + H + 2OH$$

$$S6-S7: NH_3BH_2 + H + 2OH \rightarrow NH_3BH_2OH + H + H + OH$$

$$S7: NH_3BHOH + H + H + OH \rightarrow NH_3BHOH + OH + H_2\uparrow$$

$$S7-S8: NH_3BHOH + OH \rightarrow NH_3BHO + H + OH$$

$$S8-S9: NH_3BHO + H + OH \rightarrow NH_3BO + H + H + OH$$

$$S9-S10: NH_3BO + H + H + OH \rightarrow NH_3BOOH + H_2\uparrow$$

© 2025 Wiley-VCH GmbH

15213757, 2025, 0, Downloaded from https://onlinelibrary.wiley.com/doi/10.1002/ange.202423626. By WUHAN UNIVERSITY OF TECHNOLOGY, Wiley Online Library on [30/03/2025]. See the Terms and Conditions (https://onlinelibrary.wiley.com/terms-and-conditions) on Wiley Online Library for rules of use; OA articles are governed by the applicable Creative Commons License

Table 1: Substrate scope of the selective hydrogenation of nitroaromatics to Aniline.

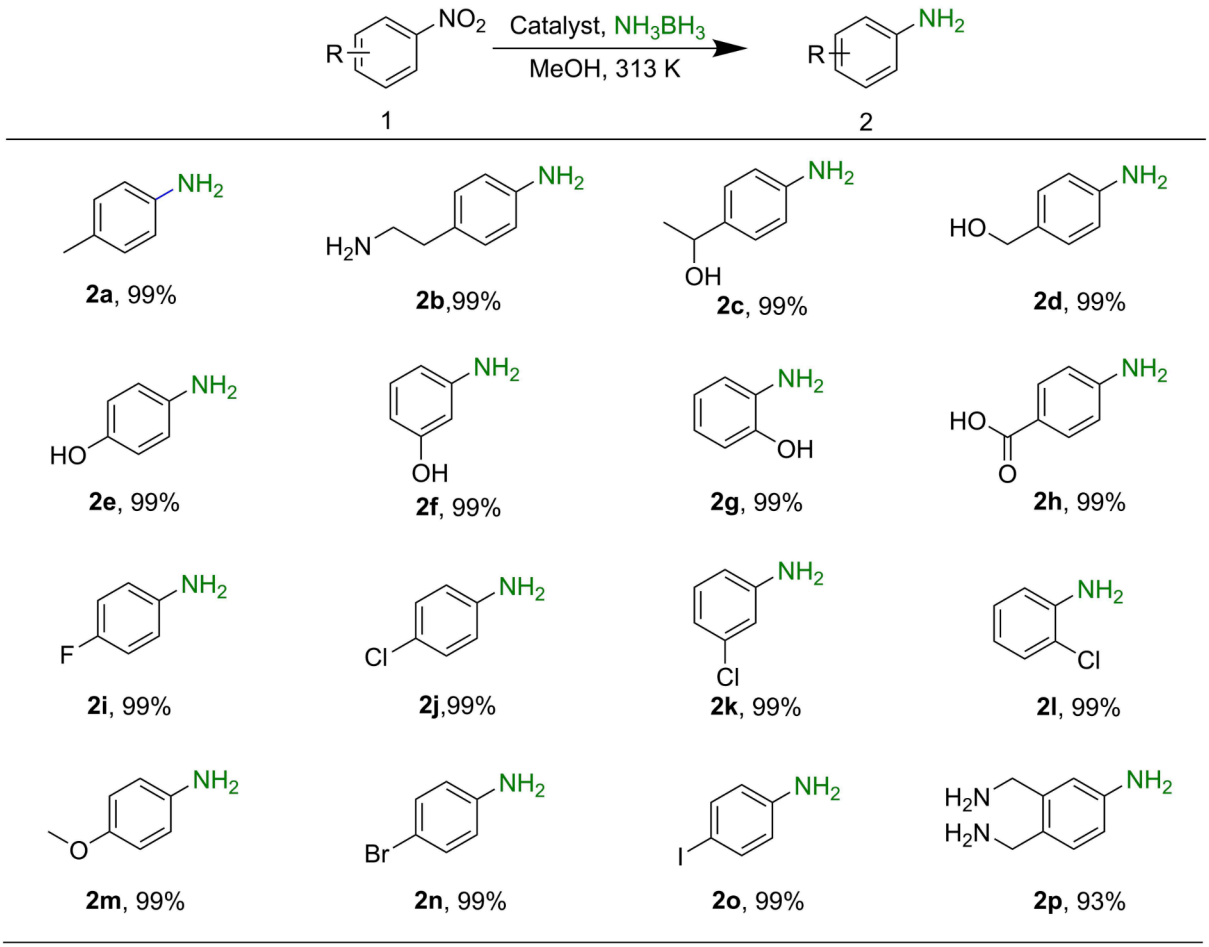

Reaction condition: $Ru_{1+n}Co_1$-TiO_2 10 mg, substrate 1 mmol, NH_3BH_3 92 mg, CH_3OH 2 mL, H_2O 0.1 g, 313 K, 4 h.

$$S10 - S11: \ NH_3BOOH \rightarrow \ NH_4BO_2$$

Figure 5e showed the ΔE for each step of hydrogen generation from AB and H_2O over the $Ru_{1+n}Co_1$-TiO_2 catalyst . The ΔE of 0.58 eV for O–H bond breaking of H_2O molecules in S3–S4 was comparable to the ΔE of 0.59 eV for B–H bond breaking in S5–S6 and was also higher than that of the other subsequent steps, suggesting that O–H and B–H bond breaking were common decisive speed steps in the AB hydrolysis process. By comparing the adsorption energy barriers of the AB hydrolysis reaction over different catalysts, it was found that the energy barriers for each step over the $Ru_{1+n}Co_1$-TiO_2 were the lowest compared to $Ru_{1+n}Cu_1$-TiO_2 and Ru_n-TiO_2 (Figure S41~43). Thus, the bimetallic-ternary-structured catalyst $Ru_{1+n}Co_1$-TiO_2 was the optimal structure with low energy barriers for efficient AB hydrolysis.

To further reveal the role of the catalyst in the AB-TH to nitrobenzene reaction, additional characterization and DFT theoretical studies were carried out. Firstly, H_2-TPD of the $Ru_{1+n}Co_1$-TiO_2 and $Ru_{1+n}Cu_1$-TiO_2 catalysts was investigated to gain insight into hydrogen activation process (Figure S44). The peak intensity of $Ru_{1+n}Co_1$-TiO_2 at low temperatures (84, 153 °C) was lower than that of $Ru_{1+n}Cu_1$-TiO_2, indicating that $Ru_{1+n}Co_1$-TiO_2 was more capable of adsorbing hydrogen, which facilitated the hydrogenation process. The peak of $Ru_{1+n}Co_1$-TiO_2 at high temperature of 305 °C in the H_2 desorption profiles was attributed to spillover hydrogen, indicating that $Ru_{1+n}Co_1$-TiO_2 had a stronger hydrogen adsorption capacity and was more likely to transfer H^- from AB to nitrobenzene. Considering that the key step in the hydrogenation of nitrobenzene over catalysts was the decomposition of NO_2* into NO*, the generation of the intermediate during the hydrogenation were monitored by in situ Raman spectroscopy to explore the catalytic mechanism. As shown in Figure 5f and Figure S45, the in situ Raman spectrum in the nitrobenzene reduction reaction with AB as hydrogen donors showed three prominent vibrational peaks of NO* at 1242, 1346, 1399 cm^{-1}. Obviously, the peaks appeared at 2 min of the reaction and the peak intensity of 1346 cm^{-1} decreased significantly, and the peak intensity of 1399^{-1} increased slightly with time, indicating that the catalyst had a strong ability to crack NO_2. The peak intensity of $Ru_{1+n}Cu_1$-TiO_2 at 1346 cm^{-1} began to weaken, and the peak intensity of Ru_n-TiO_2 at 1346 cm^{-1} was basically unchanged, and the degree

© 2025 Wiley-VCH GmbH

15213757, 2025, 0, Downloaded from https://onlinelibrary.wiley.com/doi/10.1002/ange.202423626. By WUHAN UNIVERSITY OF TECHNOLOGY, Wiley Online Library on [30/03/2025]. See the Terms and Conditions (https://onlinelibrary.wiley.com/terms-and-conditions) on Wiley Online Library for rules of use; OA articles are governed by the applicable Creative Commons License

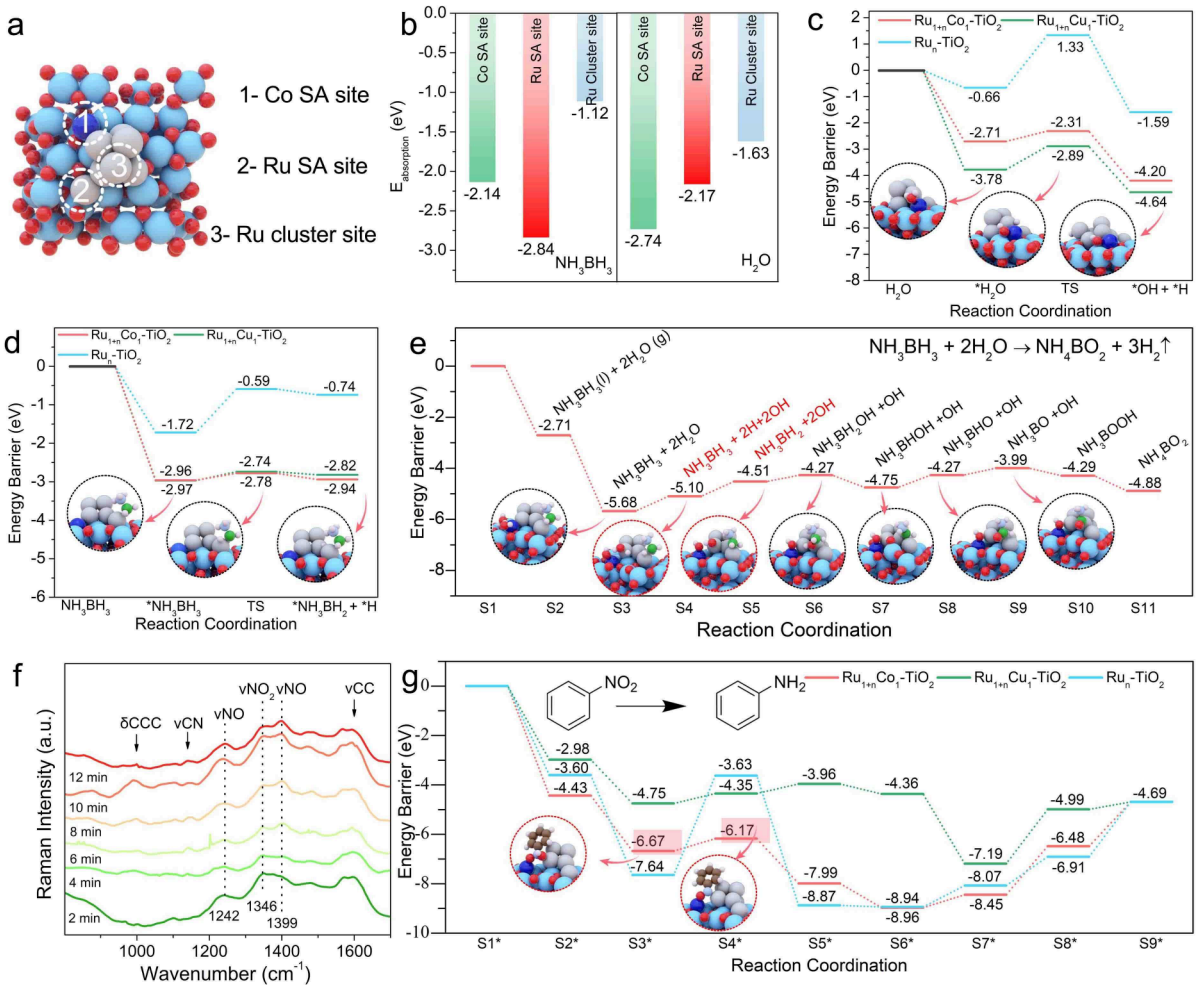

Figure 5. (a) Schematic diagram of the optimized adsorption sites. The adsorption energy $E_{absorption}$ of (b) AB and H_2O at Co SA site, Ru SA site, Ru Cluster site. Free energies and corresponding transition states for (c) H_2O and (d) AB on $Ru_{1+n}Co_1$-TiO_2, $Ru_{1+n}Cu_1$-TiO_2 and Ru_n-TiO_2. (e) The free energy diagrams of AB hydrolysis over $Ru_{1+n}Co_1$-TiO_2 catalyst. (f) In situ Raman spectra of $Ru_{1+n}Co_1$-TiO_2 applied in the hydrogenation nitrobenzene at different times. (g) The free energy diagrams of nitrobenzene hydrogenation to aniline over $Ru_{1+n}Co_1$-TiO_2 catalyst..

of peak change of both $Ru_{1+n}Cu_1$-TiO_2 and Ru_n-TiO_2 was not as pronounced as that of the $Ru_{1+n}Co_1$-TiO_2 catalyst, which suggested that the ability of $Ru_{1+n}Cu_1$-TiO_2 and Ru_n-TiO_2 to crack NO_2 was not as strong as that of $Ru_{1+n}Co_1$-TiO_2. Therefore, the catalytic activity of $Ru_{1+n}Cu_1$-TiO_2 and Ru_n-TiO_2 was also lower than that of $Ru_{1+n}Co_1$-TiO_2, which also corresponded to the results of the catalytic experiments.To gain insight into the influence on the electronic structure of catalysts, the Local density of states (LDOS) and the average d-band center position were calculated (Figure S46). The d-band center of $Ru_{1+n}Co_1$-TiO_2 (0.806 eV) far from fermi level optimized the desorption of H^- and hydrogenation products compare with $Ru_{1+n}Cu_1$-TiO_2 (0.701 eV) and Ru_n-TiO_2 (0.647 eV).

Figure 5g showed the energy barriers for each step in the hydrogenation of nitrobenzene to amine compounds over different catalysts. The corresponding model was shown in Figure S47~49. Obviously, the step S3* to S4* (C_6H_5+NOOH→C_6H_5+NO+OH) over Ru_n-TiO_2 had a highest energy barrier (4.01 eV), making it an inefficient hydrogenation pathway. The introduction of heterogeneous Co SA had significantly optimized the structure of the active site for $Ru_{1+n}Co_1$-TiO_2 catalyst, which consequently had the lowest activation energy (0.5 eV) for S3* to S4*, thus significantly improved the efficiency of the reaction.

In addition, solvent effects calculation tests were performed. As shown in Figure S50 and S51, in the case of NH_3BH_3, we set the relative permittivity (dielectric constant) as 80.0, which corresponded to water, reflecting its experimental solvation environment. For the nitrobenzene hydrogenation reaction, we considered a dielectric constant of 32.7, corresponding to methanol, based on the solvent used in the experimental conditions. The results showed that incorporating solvation effects had minimal impact on the free energy profiles compared to calculations without solvation. The impact of solvent effects using VASP Sol code was further assessed and we founded that their influence on our overall findings was relatively small. Therefore, solvent effects did not significantly change the

© 2025 Wiley-VCH GmbH

15213757, 2025, 0, Downloaded from https://onlinelibrary.wiley.com/doi/10.1002/ange.202423626. By WUHAN UNIVERSITY OF TECHNOLOGY, Wiley Online Library on [30/03/2025]. See the Terms and Conditions (https://onlinelibrary.wiley.com/terms-and-conditions) on Wiley Online Library for rules of use; OA articles are governed by the applicable Creative Commons License

discussion or interpretation of the catalytic mechanism in this study.

Conclusion

We successfully synthesized bimetallic-ternary-structured catalysts with Ru, Co SAs and Ru clusters on TiO_2 support through a simple impregnation reduction approach. The $Ru_{1+n}Co_1$-TiO_2 catalyst exhibited excellent catalytic activity for the hydrogen generation from AB hydrolysis, achieving superior *TOF* values of 2716 min^{-1}. Remarkably, a conspicuous synergistic effect was observed in TH process between Co and Ru of $Ru_{1+n}Co_1$-TiO_2 catalysts. The preparation of aniline by hydrogenation of nitrobenzene was carried out at 313 K with 99 % conversion in 4 h by in situ H^- from AB. It was well tolerated to a wide range of nitrobenzene derivative and efficiently converted to the corresponding aniline derivative with high conversion. Experiments and DFT simulations revealed that Co SA and Ru SA sites remarkably boosted the O–H cleavage and the broken of B–H, transformed H^- for nitrobenzene hydrogenation on Ru clusters and Co SA. This work not only contributes valuable insights towards the design of bimetallic-ternary-structured catalysts with multifunctional active sites for efficient hydrogen production, but also showcases the potential for the development of safe, efficient, and sustainable hydrogen technologies using chemical hydrogen storage materials.

Experimental Section

Experimental Procedures are provided in the Supporting Information.

Author Contributions

J. Shen, M. Tang and S. Guan. designed the project, carried out the experiments, collected the data and prepared the manuscript for publication. Z. Shi. carried out the calculations. Y. Shi, R. Li and J. Yang conducted the experiments, provided suggestions. Z. Zhuang and Y. Dou. carefully revised the manuscript. S. Guan, D. He, B. Liu, and D. Wang conducted project administration.

Acknowledgements

This work was supported by the National Key R&D Program of China (2023YFA1506801), the National Natural Science Foundation of China (22325101, 22171157, 22388102, 22409112), Beijing Natural Science Foundation (Z240027), and the China Postdoctoral Science Foundation (No. 2024M761601). We thank the 1W1B beamlines of Beijing Synchrotron Radiation Facility (BSRF) and the BL11B station of Shanghai Synchrotron Radiation Facility (SSRF) measurement for providing beam time to support this work. We thank the Anhui Absorption Spectroscopy AnalysisInstrument Co, Ltd. for XAFS measurements and analysis.

Conflict of Interest

The authors declare no conflict of interest.

Data Availability Statement

The data that support the findings of this study are available from the corresponding author upon reasonable request.

Keywords: Transfer Hydrogenation · AB Hydrolysis · Nitrobenzene Hydrogenation · Synergistic Catalysis · Bimetallic-Ternary-Structured Catalysts

[1] a) S. Lau, D. Gasperini, R. L. Webster, *Angew. Chem. Int. Ed.* **2021**, *60*, 14272; b) A. Han, J. Zhang, W. Sun, W. Chen, S. Zhang, Y. Han, Q. Feng, L. Zheng, L. Gu, C. Chen, Q. Peng, D. Wang, Y. Li, *Nat. Commun.* **2019**, *10*, 3787; c) M. Tang, J. Shen, Y. Wang, Y. Zhao, T. Gan, X. Zheng, D. Wang, B. Han, Z. Liu, *Nat. Commun.* **2024**, *15*, 5630.

[2] a) J. Li, T. Cai, Y. Feng, X. Liu, N. Wang, Q. Sun, *Science China Chemistry* **2024**, *67*, 2911; b) H.-X. Wang, W. L. Toh, B. Y. Tang, Y. Surendranath, *Nat. Catal.* **2023**, *6*, 351.

[3] J. Zheng, X. Liu, P. Xu, P. Liu, Y. Zhao, J. Yang, *Int. J. Hydrogen Energy* **2012**, *37*, 1048.

[4] R. Sang, C. A. M. Stein, T. Schareina, Y. Hu, A. Léval, J. Massa, V. Turan, P. Sponholz, D. Wei, R. Jackstell, H. Junge, M. Beller, *Nat. Commun.* **2024**, *15*, 7268.

[5] a) D. Liu, C. Zhou, Z. Yang, G. Wang, C. Kong, B. Liu, *Mater. Chem. Front.* **2023**, *7*, 4339; b) Q. Yao, X. Zhang, Z.-H. Lu, Q. Xu, *Coord. Chem. Rev.* **2023**, *493*, 215302; c) J. Yao, Z. Wu, H. Wang, F. Yang, J. Ren, Z. Zhang, *J. Energy Chem.* **2022**, *74*, 218.

[6] a) C. Wan, R. Li, J. Wang, D. g. Cheng, F. Chen, L. Xu, M. Gao, Y. Kang, M. Eguchi, Y. Yamauchi, *Angew. Chem. Int. Ed.* **2024**, *63*, e202404505; b) Y. Meng, Q. Sun, T. Zhang, J. Zhang, Z. Dong, Y. Ma, Z. Wu, H. Wang, X. Bao, Q. Sun, J. Yu, *J. Am. Chem. Soc.* **2023**, *145*, 5486; c) S. Guan, Y. Liu, H. Zhang, R. Shen, H. Wen, N. Kang, J. Zhou, B. Liu, Y. Fan, J. Jiang, B. Li, *Adv. Sci.* **2023**, 2300726; d) J. Li, Q. Guan, H. Wu, W. Liu, Y. Lin, Z. Sun, X. Ye, X. Zheng, H. Pan, J. Zhu, S. Chen, W. Zhang, S. Wei, J. Lu, *J. Am. Chem. Soc.* **2019**, *141*, 14515.

[7] X. Chu, G. Zhou, M. Pang, H. Zhang, *Eur. J. Org. Chem.* **2023**.

[8] a) W. Zhao, H. Li, H. Zhang, S. Yang, A. Riisager, *Green Energy & Environ.* **2023**, *8*, 948; b) L. Winner, W. C. Ewing, K. Geetharani, T. Dellermann, B. Jouppi, T. Kupfer, M. Schafer, H. Braunschweig, *Angew. Chem. Int. Ed.* **2018**, *57*, 12275.

[9] A. Hajari, B. Roy, V. Kumar, A. Bishnoi, P. Sharma, *ChemistrySelect* **2021**, *6*, 1276.

[10] a) J. Yang, Z. Yang, J. Li, H. Gang, D. Mei, D. Yin, R. Deng, Y. Zhu, X. Li, N. Wang, S. M. Osman, Y. Yamauchi, *Mater. Horiz.* **2024**, *11*, 2032; b) L. Bian, L. Liang, Y. Fan, X. Liu, F. Liang, Q. Peng, S. Han, L. Liu, B. Liu, *J. Colloid Interface Sci.* **2024**, *671*, 543.

[11] a) S. Özkar, *Int. J. Hydrogen Energy* **2024**, *54*, 327; b) N. Wang, Q. Sun, T. Zhang, A. Mayoral, L. Li, X. Zhou, J. Xu, P. Zhang, J. Yu, *J. Am. Chem. Soc.* **2021**, *143*, 6905.

© 2025 Wiley-VCH GmbH

15213757, 2025, 0, Downloaded from https://onlinelibrary.wiley.com/doi/10.1002/ange.202423626. By WUHAN UNIVERSITY OF TECHNOLOGY, Wiley Online Library on [30/03/2025]. See the Terms and Conditions (https://onlinelibrary.wiley.com/terms-and-conditions) on Wiley Online Library for rules of use; OA articles are governed by the applicable Creative Commons License

[12] a) S. Alemdar, A. Basak, O. Metin, *ACS Appl. Mater. Interfaces* **2023**, *15*, 48096; b) R. Shen, Y. Liu, H. Wen, X. Wu, G. Han, X. Yue, S. Mehdi, T. Liu, H. Cao, E. Liang, B. Li, *Small* **2022**, *18*, 2105588.
[13] a) D. Patra, R. Ganesan, B. Gopalan, *Int. J. Hydrogen Energy* **2021**, *46*, 25486; b) Y. Yuan, L. Sun, G. Wu, Y. Yuan, W. Zhan, X. Wang, X. Han, *Inorg. Chem.* **2020**, *59*, 2104.
[14] a) S. Guan, Z. Yuan, S. Zhao, Z. Zhuang, H. Zhang, R. Shen, Y. Fan, B. Li, D. Wang, B. Liu, *Angew. Chem. Int. Ed.* **2024**, e202408193; b) S. Guan, Z. Yuan, Z. Zhuang, H. Zhang, H. Wen, Y. Fan, B. Li, D. Wang, B. Liu, *Angew. Chem. Int. Ed.* **2023**, *63*, 202316550.
[15] a) J. Li, Y. Feng, X. Li, T. Zhang, X. Liu, N. Wang, Q. Sun, *ACS Catal.* **2024**, 14665; b) S. Chen, B. Gong, J. Gu, Y. Lin, B. Yang, Q. Gu, R. Jin, Q. Liu, W. Ying, X. Shi, W. Xu, L. Cai, Y. Li, Z. Sun, S. Wei, W. Zhang, J. Lu, *Angew. Chem. Int. Ed.* **2022**, 202211919.
[16] a) Z. Zhang, J. Wang, X. Ge, S. Wang, A. Li, R. Li, J. Shen, X. Liang, T. Gan, X. Han, X. Zheng, X. Duan, D. Wang, J. Jiang, Y. Li, *J. Am. Chem. Soc.* **2023**, *145*, 22836; b) R. Li, Z. Zhang, X. Liang, J. Shen, J. Wang, W. Sun, D. Wang, J. Jiang, Y. Li, *J. Am. Chem. Soc.* **2023**, *145*, 16218–16227.
[17] a) Y. Wang, F. Ma, G. Zhang, J. Zhang, H. Zhao, Y. Dong, D. Wang, *Nano Res.* **2024**, *17*, 9397; b) L. Wang, J. Wu, S. Wang, H. Liu, Y. Wang, D. Wang, *Nano Res.* **2023**, *17*, 3261.
[18] a) X. Yan, D. Liu, P. Guo, Y. He, X. Wang, Z. Li, H. Pan, D. Sun, F. Fang, R. Wu, *Adv. Mater.* **2023**, *35*, 2210975; b) A. R. Poerwoprajitno, L. Gloag, J. Watt, S. Cheong, X. Tan, H. Lei, H. A. Tahini, A. Henson, B. Subhash, N. M. Bedford, B. K. Miller, P. B. O'Mara, T. M. Benedetti, D. L. Huber, W. Zhang, S. C. Smith, J. J. Gooding, W. Schuhmann, R. D. Tilley, *Nat. Catal.* **2022**, *5*, 231; c) M. Tang, J. Shen, F. Zhang, Y. Zhao, T. Gan, W. Zeng, R. Li, D. Wang, B. Han, Z. Liu, *Angew. Chem. Int. Ed.* **2024**, e202416436; d) T. Gan, D. Wang, *Nano Res.* **2023**, *17*, 18.
[19] W. Ni, J. L. Meibom, N. U. Hassan, M. Chang, Y.-C. Chu, A. Krammer, S. Sun, Y. Zheng, L. Bai, W. Ma, S. Lee, S. Jin, J. S. Luterbacher, A. Schüler, H. M. Chen, W. E. Mustain, X. Hu, *Nat. Catal.* **2023**, *6*, 773.
[20] a) Y. Zhang, P. Luo, J. Qi, H. Lu, L. Wang, Y. Wu, *New J. Chem.* **2024**, *48*, 8371; b) E. Punzi, X. T. Nguyen, E. Pitzalis, A. Mandoli, M. Onor, M. Marelli, L. Poggini, G. Tuci, G. Giambastiani, C. Evangelisti, *ACS Applied Nano Materials* **2024**, *7*, 6916–6926.

Manuscript received: December 3, 2024
Accepted manuscript online: February 25, 2025
Version of record online: ■■, ■■

15213757, 2025, 0, Downloaded from https://onlinelibrary.wiley.com/doi/10.1002/ange.202423626. By WUHAN UNIVERSITY OF TECHNOLOGY, Wiley Online Library on [30/03/2025]. See the Terms and Conditions (https://onlinelibrary.wiley.com/terms-and-conditions) on Wiley Online Library for rules of use; OA articles are governed by the applicable Creative Commons License

© 2025 Wiley-VCH GmbH

Forschungsartikel

Nitrobenzene Hydrogenation

J. Shen, M. Tang, Z. Shi, S. Guan,* Y. Shi, Z. Zhuang, R. Li, J. Yang, D. He,* B. Liu,* Y. Dou, D. Wang* **e202423626**

Efficient Generation of Negative Hydrogen with Bimetallic-Ternary-Structured Catalysts for Nitrobenzene Hydrogenation

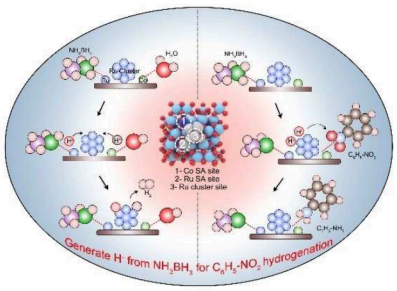

The bimetallic-ternary-structured catalysts $Ru_{1+n}Co_1$-TiO_2 catalysts exhibited highest activity for hydrogen evolution form AB hydrolysis with a TOF value of 2716 min^{-1} and achieved >90% yields within 3–4 hours using AB as H in converting nitrobenzene to anilines.

15213757, 2025, 0, Downloaded from https://onlinelibrary.wiley.com/doi/10.1002/ange.202423626. By WUHAN UNIVERSITY OF TECHNOLOGY, Wiley Online Library on [30/03/2025]. See the Terms and Conditions (https://onlinelibrary.wiley.com/terms-and-conditions) on Wiley Online Library for rules of use; OA articles are governed by the applicable Creative Commons License

© 2025 Wiley-VCH GmbH